electronics

MDPI

Article

State of Health Prediction of Lithium-Ion Batteries Based on the Discharge Voltage and Temperature

Yanru Yang [1], Jie Wen [1,*], Yuanhao Shi [1] and Jianchao Zeng [2,*]

[1] School of Electrical and Control Engineering, North University of China, Taiyuan 030051, China; yanruyang521@gmail.com (Y.Y.); yhshi@nuc.edu.cn (Y.S.)
[2] School of Data Science and Technology, North University of China, Taiyuan 030051, China
* Correspondence: wenjie@nuc.edu.cn (J.W.); zjc@nuc.edu.cn (J.Z.)

Abstract: Accurate state of health (SOH) prediction of lithium-ion batteries is essential for battery health management. In this paper, a novel method of predicting the SOH of lithium-ion batteries based on the voltage and temperature in the discharging process is proposed to achieve the accurate prediction. Both the equal voltage discharge time and the temperature change during the discharge process are regarded as health indicators (HIs), and then, the Pearson and Spearman relational analysis methods are applied to evaluate the relevance between HIs and SOH. On this basis, we modify the relevance vector machine (RVM) to a multiple kernel relevance vector machine (MKRVM) by combining Gaussian with sigmoid function to improve the accuracy of SOH prediction. The particle swarm optimization (PSO) is used to find the optimal weight and kernel function parameters of MKRVM. The aging data from NASA Ames Prognostics Center of Excellence are used to verify the effectiveness and accuracy of the proposed method in numerical simulations, whose results show that the MKRVM method has higher SOH prediction accuracy of lithium-ion batteries than the relevant methods.

Keywords: lithium-ion battery; state of health; multiple kernel relevance vector machine

Citation: Yang, Y.; Wen, J.; Shi, Y.; Zeng, J. State of Health Prediction of Lithium-Ion Batteries Based on the Discharge Voltage and Temperature. *Electronics* **2021**, *10*, 1497. https://doi.org/10.3390/electronics10121497

Academic Editors: Inhee Lee and Sara Deilami

Received: 23 April 2021
Accepted: 18 June 2021
Published: 21 June 2021

1. Introduction

Lithium-ion batteries have been widely used in aviation [1], electronic technology, and other fields [2] due to the high energy density, long service life, and low self-discharge rate. However, the capacity of the lithium-ion battery will degenerate after repeated charge and discharge. When the capacity of the lithium-ion battery degenerates a threshold, the lithium-ion battery should be replaced to ensure system safety and avoid the occurrence of serious accidents. Therefore, we need to understand and take it as a guide to provide security for the system operation, which makes it of great significance to study the state of health (SOH) of lithium-ion batteries [3].

The prediction of SOH is still facing great challenges. The prediction methods of SOH for lithium-ion batteries are mainly divided into three types: model-based method [4], data-driven method [5,6], and fusion method [7]. The model-based method is mainly to establish a mathematical model of describing the failure of the battery through the prior knowledge in the battery degradation e.g., equivalent circuit model [8], empirical model [9], electrochemical model [10], etc. The data-driven method uses machine learning techniques (such as Gaussian process regression (GPR) [11,12], support vector regression (SVR) [13], relevance vector machine (RVM) [14,15], artificial neural network (ANN), deep learning [16,17], and so on) to predict the SOH based on the battery degradation data. The prediction can be divided into direct prediction and indirect prediction. Direct prediction is to predict the SOH of lithium-ion batteries by taking capacity or internal resistance as a health indicator (HI). For example, Qu et al. [18] proposed complete ensemble empirical mode decomposition with adaptive noise based on capacity and combined long short-term memory with particle swarm optimization (PSO) as well as an attention mechanism for

SOH monitoring of the lithium-ion battery. In particular, the model design of the deep learning method is complex, which requires a lot of training data and large-scale computer computing ability, and there are many parameters to learn, such that hardware with strong calculation capability is needed. To improve the computation speed and prediction accuracy, Qin et al. [19] used SVR to predict the SOH, and PSO is employed in obtaining the SVR kernel parameter, which can well grasp the trend of SOH. However, because capacity measurement is time-consuming and requires expensive instruments [20] and obtaining real-time capacity is a challenging technology, the data-driven indirect prediction method has been widely used in the SOH prediction of lithium-ion batteries. In other words, the indirect extraction of useful information from the voltage, current, and temperature changes of lithium-ion batteries can reflect capacity degradation to achieve SOH prediction. Widodo et al. [21] took the discharge voltage sample entropy as HI and used SVR and RVM as the prediction model of SOH respectively and shown that RVM had better prediction performance than SVR. Compared with SVR, RVM based on Bayesian theory has more sparsity and less computation of kernel function. Liu et al. [22] selected the time of the equal voltage interval during the constant current charging process as the HI. Then, by using the Pearson and Spearman methods, the correlation relationship between the HI and SOH is evaluated. In addition, Yang et al. [23] extracted four HIs to reflect battery aging from different sides according to the charging curve, used grey correlation analysis to analyze the relationship between HIs and SOH and adjusted the covariance function of GPR to improve the prediction accuracy of SOH. RVM is a Bayesian sparse kernel technique with simple hyperparameters and can have probabilistic results. So, RVM has been widely used in SOH prediction. Liu et al. [24] used the RVM method to model the extracted HIs after Box–Cox transformation to predict the SOH and remaining useful life (RUL) of lithium-ion batteries. Moreover, multiple kernel relevance vector machine (MKRVM) has better generalization performance than the single kernel method [25,26]. Zhang et al. [27] used capacity as HI and established an MKRVM model based on the capacity data of empirical mode decomposition; the MKRVM method can accurately predict the future capacity of the battery.

Recently, the fusion model has been proposed, which combines the advantages of two or more methods widely used in the SOH prediction of lithium-ion batteries [28,29]. Dong et al. [30] proposed SVR and particle filter (PF) for the SOH monitoring and RUL prediction, and the models for battery SOH monitoring based on SVR-PF are developed with novel capacity degradation parameters introduced to determine battery health in real time.

However, the temperature change during the discharge process is not considered in the above-mentioned works. Temperature and aging are the two main factors affecting the reliability and safety of lithium-ion batteries [31]. The change of temperature has a great influence on the electrochemical reaction inside the battery. Ma et al. [32] have analyzed the effect of temperature on the degradation of lithium-ion batteries, while Ruiz et al. [33] systematically evaluated the impact of different charge and discharge temperatures on the long-term performance of lithium iron phosphate/graphite batteries by using variance multi-factors analysis.

In this paper, we propose a lithium-ion battery SOH prediction method that considers the partial data of voltage and temperature during the discharge process. First, considering the difficulty of capacity measurement, we utilize an indirect HIs method. Moreover, considering that the battery is not fully discharged during actual working, it will be charged when the battery is not discharged to the cut-off voltage, so partial data, the time interval of an equal discharging voltage difference (TIEDVD), and the temperature interval of an equal discharging time difference (TIEDTD) are extracted as HIs for SOH prediction. The change of voltage and temperature can reflect not only the changing trend of capacity but also the phenomenon of capacity recovery. In addition, we use the Pearson and Spearman methods for correlation analysis to measure the relationship between the extracted HIs and SOH. Due to there being a phenomenon of capacity recovery during the

battery degradation process, we utilize the global sigmoid kernel function and the local Gaussian kernel function to improve the performance of the RVM model to achieve higher accuracy of SOH prediction. Moreover, the datasets provided by NASA are used to verify the effectiveness and accuracy of the method proposed in this paper.

The remainder of this paper is organized as follows. In Section 2, the lithium-ion battery datasets, as well as the feature extraction process and correlation analysis are described. The method of MKRVM is introduced in Section 3. The experimental result verification and analysis are provided in Section 4. Finally, the conclusion is discussed in Section 5.

2. Feature Extraction and Analysis Based on Discharge Curves

In this section, the features, which can reflect the battery degradation during the discharging process, are extracted for SOH prediction.

2.1. The Definition of SOH

SOH is a significant indicator that can be used to measure the health of the lithium-ion battery, which leads to the accurate prediction of SOH being able to guide prognosis management. The SOH of lithium-ion batteries can be defined based on the capacity, internal resistance, cycle number, and so on. In this paper, SOH is defined by using the battery capacity as follows [34]:

$$SOH = \frac{C_i}{C_0} \tag{1}$$

where C_i is the capacity at the ith cycle, and C_0 is the initial capacity.

2.2. Experiment Data

The effectiveness of the MKRVM prediction model is evaluated based on the data from the data repository of the NASA Ames Prognostics Center of Excellence [35]. This datasets are collected from a battery prognostic test-bed at NASA 18650 comprising commercially available lithium-ion rechargeable batteries whose nominal capacity is 2 Ah and nominal voltage is 3.7 V [36,37]. In order to verify the effectiveness of the MKRVM, a set of batteries #5, #6, #7, and #18, and another set of batteries #54 and #55 in three different operating conditions are used in this paper. Lithium-ion batteries are run through three different operational profiles (charge, discharge, and impedance). Batteries #5, #6, #7, and #18 are tested at room temperature (24 °C). First, charging is carried out in a constant current mode at 1.5 A until the battery voltage reached 4.2 V and then continued in a constant voltage mode until the charge current dropped to 20 mA. After that, the discharge process is carried out at a constant current of 2 A until the battery voltage falls to 2.7, 2.5, 2.2, and 2.5 V for batteries #5, #6, #7, and #18, respectively. Thus, batteries #5, #6, and #7 are cycled with different depth of discharge (DoD), batteries #6 and #18 are cycled with the same DoD. However, the cycles corresponding to the failure threshold of battery #18 are much shorter than those of battery #6 due to the different types of batteries. Meanwhile, batteries #54 and #55 discharged at a constant current of 2A stop at 2.2 V and 2.5 V in a low-temperature environment (4 °C). Repeated charge and discharge cycles result in accelerated aging of batteries, and the capacity with cycle numbers are shown in Figure 1. In Figure 1b, the first point and the last point have been removed from the capacity data due to a big shift for batteries #54 and #55. For batteries #54 and #55, we can observe from Figure 1b that the battery with many local noises due to being under low temperature, batteries #54 and #55, are used to verify the extrapolation performance of the method proposed in this paper.

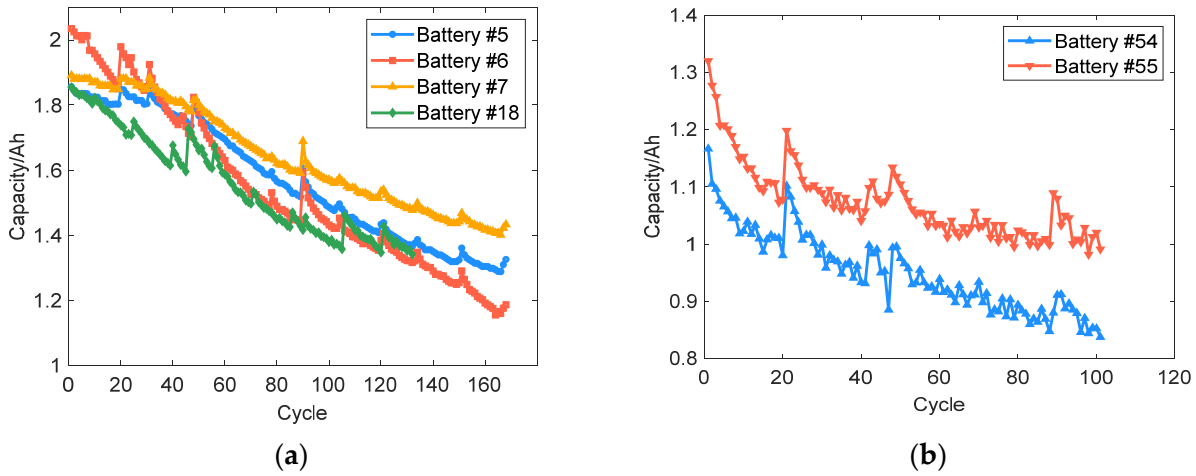

(**a**) (**b**)

Figure 1. Capacity degradation curves of batteries. (**a**) #5, #6, #7, and #18; (**b**) #54, #55.

2.3. Feature Extraction Based on Discharging Curves

Feature extraction can be regarded as an information simplification process to extract meaningful signals from the original data to reduce the input size without affecting the performance of the model. There are many factors affecting battery degradation, such as temperature, current, voltage, cyclic life, etc. Since the current is constant in the discharging process, the voltage and temperature are considered in this paper. Meanwhile, considering the battery will not start charging until the cut-off voltage, part of the data of the low state of charge (SOC) area is discarded. In addition, when the battery is open circuit and not in a working state, which with the existence of self-discharge, the battery may not be in a high SOC region during working. In addition, using partial data can reduce the calculation time and solve information redundancy. Taking the data of battery #5 as an example, the feature extraction is introduced in Figure 2, in which Figure 2a shows the voltage changing of battery #5 at different cycle numbers and Figure 2b shows the temperature changes in different cycles. It can be observed from Figure 2 that the time to reach a specific voltage is different for different cycles, and the voltage variation between 3.0 and 3.8 V covers the main information of the discharge process [38].

(1) TIEDVD: From Figure 2a, we can see that the time of different cycles in the same voltage interval is different. As the cycle of battery charge and discharge increases, the voltage drop rate is different. Taking the 150th cycle as an example, t1(150) corresponds to the time when the battery voltage reaches 3V, t2(150) corresponds to the time when the battery voltage reaches 3.8V, and TIEDVD is equal to t1–t2. The result is shown in Figure 3a,we can see that TIEDVD is consistent with the capacity change trend and local fluctuations.

(2) TIEDTD: During the time of voltage change, we also analyze the temperature change during this period. T1(150) is the point corresponding to t1(150), T2(150) is the point corresponding to t2(150), and TIEDTD is equal to T2–T1. From Figure 2b, we can see that temperature change simultaneously is not the same. So, we extract the temperature change within the same time as other HI. The normalized HIs are shown in Figure 3b, while TIEDTD and the capacity change trend show the opposite trend in this paper.

The TIEDVD and TIEDTD, which are selected from voltage and temperature, are used as inputs of the MKRVM model to obtain the SOH prediction of lithium-ion batteries.

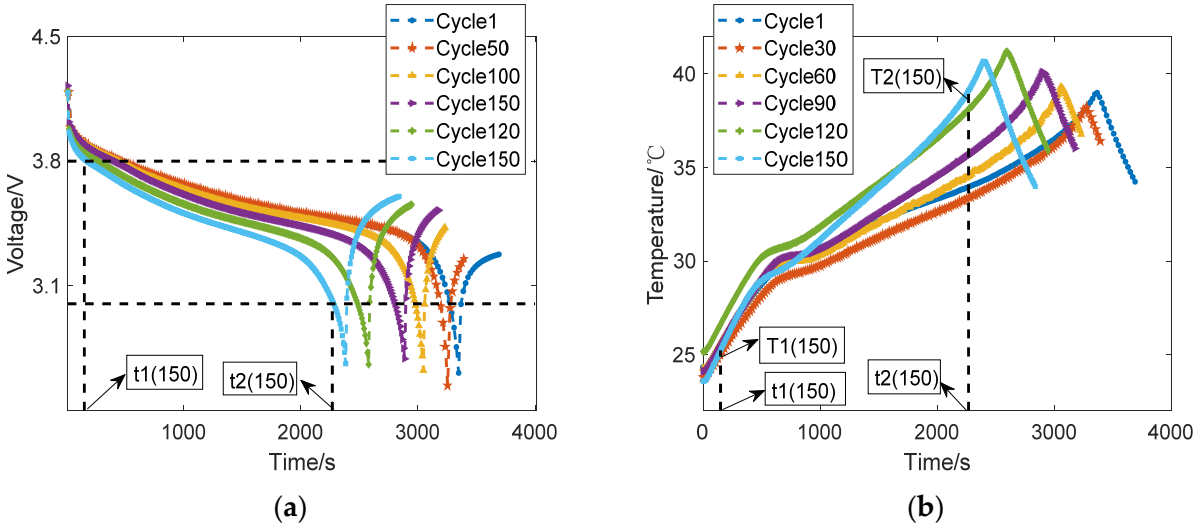

(**a**) (**b**)

Figure 2. Representations of the feature selection. (**a**) Representation of the feature selection in voltage curve; (**b**) Representation of the feature selection in temperature curve.

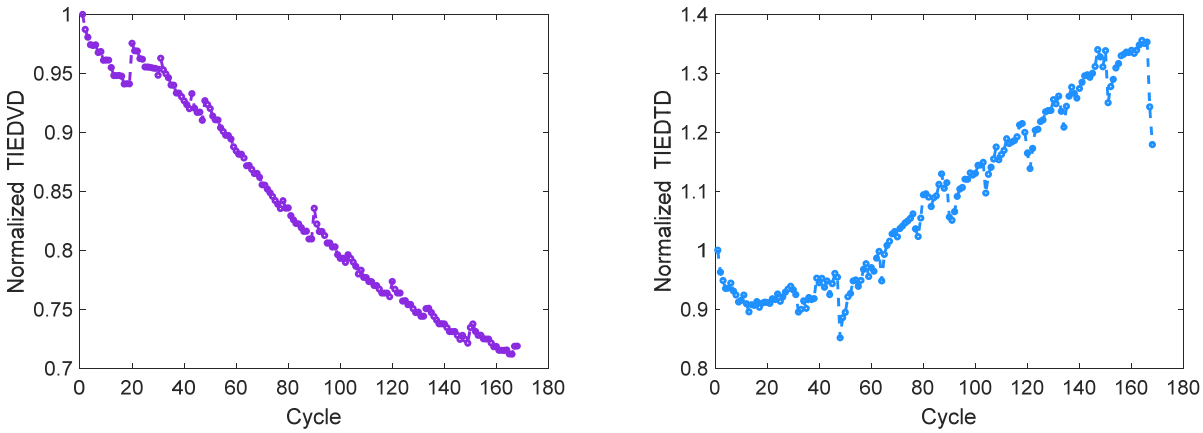

(**a**) (**b**)

Figure 3. Changes of the selected features with cycle numbers. (**a**) TIEDVD; (**b**) TIEDTD.

2.4. Feature Analysis Based on Pearson and Spearman

It can be seen from Figure 3 that the TIEDVD and the capacity degradation trend are the same. While the temperature changes within the same time, as the cycle changes, it shows the opposite trend to the capacity, and the fluctuation part corresponds to it. All the tested batteries show a similar change to that of battery #5, as shown in Figure 3. To verify the effectiveness of the extracted HIs, the correlation analysis between HIs and SOH is presented as follows.

Pearson Correlation Analysis: Assuming that there are two variables X and Y, the Pearson correlation coefficient between the two variables can be calculated by the following formula:

$$\rho_{X,Y} = \frac{cov(X,Y)}{\sigma_X \sigma_Y} = \frac{E(XY) - E(X)E(Y)}{\sqrt{E(X^2) - E^2(X)}\sqrt{E(Y^2) - E^2(Y)}} \quad (2)$$

In this paper, X is the SOH, and Y is the HI. The value of the correlation coefficient is between -1 and $+1$. The greater the absolute value of the correlation coefficient, the stronger the correlation. The correlation analysis between the HIs and SOH is shown in Table 1. It can be seen from Table 1 that the absolute values of the Pearson correlation

coefficient of HIs proposed in this paper are above 0.9, and it can be seen that HIs are strongly correlated with SOH.

Table 1. Correlation Analysis between HIs and SOH.

Battery	Pearson		Spearman	
	TIEDVD	TIEDTD	TIEDVD	TIEDTD
#5	0.9972	−0.9785	0.9983	−0.9643
#6	0.9969	−0.9513	0.9995	−0.9343
#7	0.9968	−0.9381	0.9972	−0.9175
#18	0.9973	−0.9286	0.9986	−0.9325

Spearman Correlation Analysis: Spearman uses the rank of two variables to make a linear correlation analysis, and it belongs to a non-parametric statistical method that has a wider range of applications [39,40]. Spearman's calculation formulas are as follows:

$$\rho(a,b) = 1 - \frac{6\sum d_i^2}{n(n^2-1)} \tag{3}$$

where $d_i = rg(X_I) - rg(Y_i)$, n is the number of variables, and $\rho(a,b)$ is the Spearman rank correlation coefficient. The value of the Spearman correlation coefficient is also from −1 to +1, when the absolute value of correlation is close to 1, the greater the correlation between variables X and Y.

From Table 1, one can see that the absolute value of Pearson and Spearman correlation coefficients of the TIEDVD and TIEDTD and SOH are all above 0.9. Thus, the HIs chosen in this paper are highly correlated with SOH and are effective, so that it is reasonable for building an RVM model and achieving accurate SOH predictions.

3. Methodologies

This section mainly describes the method proposed in this paper. The RVM method has been widely used in SOH prediction [41]. Compared with SVM, RVM can provide probability interpretation under the Bayesian framework, and it can also achieve a better generalization performance with fewer kernel functions. So, we use RVM and describe the MKRVM method in this section.

3.1. MKRVM

Let $\{x_i\}_{i=1,2...N}$ denote a set of input vectors, and their corresponding targets $\{t_i\}_{i=1,2...N}$, where N is the length of the training data. In this paper, x_i represents HI, and SOH is denoted as t_i. The RVM learns the relationship between the target variable t and the input variable x to accurately predict $\hat{t}$ through $\hat{x}$. We assume the relationship between the input vector x and the true output vector t can be written as:

$$t_i = y(x_i, w) + \varepsilon_i \tag{4}$$

$$y_i = \sum_{i=1}^{N} w_i K(x, x_i) \tag{5}$$

In Equation (4), ε_i is the independent errors following $\varepsilon_i \sim N(0, \sigma^2)$. In Equation (5), $K(x, x_i)$ is the kernel function, and $w_i = (w_1, w_2, \ldots, w_N)^T$ is the corresponding weight, and then, the likelihood can be written as:

$$p\left(t\middle|w,\sigma^2\right) = \left(2\pi\sigma^2\right)^{-N/2} \exp\left\{-\frac{1}{2\sigma^2}\|t-\Phi w\|^2\right\} \tag{6}$$

where Φ is an $N \times (N+1)$ design matrix with $\Phi = [\phi(x_1), \phi(x_2), \ldots \phi(x_n)]^T$ and $\Phi(x_n) = [1, K(x_n, x_1), K(x_n, x_2), \ldots K(x_n, x_n)]^T$.

To prevent the over-fitting problem caused by maximizing the likelihood, in which a zero-mean Gaussian prior distribution N over w is defined as:

$$p(w|\eta) = \prod_{i=1}^{N} N\left(w_i \middle| 0, \eta_i^{-1}\right) \tag{7}$$

With η, a vector of $N+1$ hyperparameters, which is also the target of our optimization. Then, the posterior distribution over the weights is given the data from Bayes' rule:

$$p\left(w, \eta, \sigma^2 \middle| t\right) = (2\pi)^{-(N+1)/2} |\Sigma|^{-1/2} \times \exp\left\{-\frac{1}{2}(w-\mu)^T \Sigma^{-1} (w-\mu)\right\} \tag{8}$$

where the posterior covariance matrix and mean vector are:

$$\Sigma = \left(\sigma^{-2}\Phi^T\Phi + \theta\right), with \theta = diag(\eta) \tag{9}$$

$$\mu = \sigma^{-2}\Sigma\Phi^T x \tag{10}$$

Then, to obtain the value of η and σ^2, whose most-probable (MP) values are calculated with an iterative re-evaluation algorithm:

$$\eta_i^{new} = \frac{\gamma_i}{\mu_i^2} \tag{11}$$

$$\left(\sigma^2\right)^{new} = \frac{|t - \Phi\mu|^2}{N - \Sigma_i \gamma_i} \tag{12}$$

$$\gamma_i = 1 - \eta_i \Sigma_{ii} \tag{13}$$

With a new input $\hat{x}$, the corresponding output distribution can be given as follows:

$$p(\hat{t}|t) = \int p\left(\hat{t} \middle| w, \sigma_{MP}^2\right) p\left(w \middle| t, \eta_{MP}, \sigma_{MP}^2\right) dw \tag{14}$$

where the mean and the variance are respectively:

$$\hat{y} = \mu^T \phi(\hat{x}) \tag{15}$$

$$\sigma^2 = \sigma_{MP}^2 + \phi(\hat{x})^T \Sigma \phi(\hat{x}) \tag{16}$$

It can be seen from Equation (14) that the selection of the kernel function is very important for the establishment of the model. Compared with a single kernel function, a multi-kernel functions has higher flexibility. The generalization ability of a single kernel function is weak. Combining multiple different kernel functions to get better characteristics is the basic idea of a mixed kernel function. Therefore, the Gaussian kernel function and sigmoid function as the hybrid kernel functions of MKRVM, and the expression of the mixed kernel function is:

$$K = \sum_{j=1}^{n} m_j K_j, m_j \geq 0, \sum_{j=1}^{n} m_j = 1 \tag{17}$$

where K_j is the basic kernel function, and m_j is the weight coefficient, that is, the combination coefficient.

In this paper, a mixed kernel function of Gaussian and sigmoid is used. The Gaussian kernel function has strong nonlinear processing capabilities, and it is often used as a kernel function:

$$K_1(x, x_n) = \exp\left(-\frac{\|x - x_n\|^2}{2d^2}\right) \tag{18}$$

Among them, d is the bandwidth, which is used to control the local scope of the Gaussian kernel function.

The sigmoid kernel function from the neural network has been proved to have good classification performance [42], and it can be expressed as:

$$K_2(x, x_n) = \tan h\left(tx^T x_n + c\right) \tag{19}$$

where t is a scalar, which is an amplitude adjustment parameter of the input data, and c is a displacement parameter that controls the mapping threshold. Among them, the combination coefficient m and the kernel function parameters d, c are to be optimized and determined. In order to determine the optimal kernel function weights and kernel function parameters, PSO is applied to optimize them, so as to reduce the model generalization error and prevent over-fitting.

3.2. PSO

PSO is a global random search algorithm based on swarm intelligence by simulating the migration and clustering behavior of birds in the process of foraging. It has been widely used in function optimization, neural network training, fuzzy system control, and other application areas.

The procedures of the PSO algorithm are as follows:

Step 1. Initialize the particle swarm position and speed.
Step 2. Calculate the fitness value of each particle.
Step 3. Compare the current position of each particle with the historical optimal position fitness, and the optimal position is regarded as the individual optimal position.
Step 4. Compare the optimal position of each particle with the optimal individual position in the group, and the optimal position is obtained as the global optimal position.
Step 5. Update particle speed and position.

$$v_i^{k+1} = v_i^k + c_1\lambda_1\left(p_i^k - x_i^k\right) + c_2\lambda_2\left(g_i^k - x_i^k\right) \tag{20}$$

$$x_i^{k+1} = x_i^l + v_i^{k+1} \tag{21}$$

where v_i^k, x_i^k, and p_i^k are the particle velocity, current location, and best location in the history of particle i when the iteration is k, respectively. c_1 and c_2 are accelerating factors, λ_1 and λ_2 are random numbers between 0 and 1.

With this algorithm, the optimal parameters of MKRVM can be found automatically, and the prediction accuracy of the model can be further improved. The PSO algorithm flow chart is shown in Figure 4.

3.3. SOH Prediction Based on the PSO-MKRVM

The flow chart of SOH prediction based on MKRVM is shown in Figure 5. First, we extract the corresponding HIs from the lithium-ion battery discharge data, perform correlation analysis, and then use the extracted HIs as the inputs of the MKRVM model for training; finally, the effectiveness of the proposed method is verified by the test sets. Here, the following experiments are based on Matlab 2019a on a laptop with an Inter Pentium 2.6 GHz (i7-9750H).

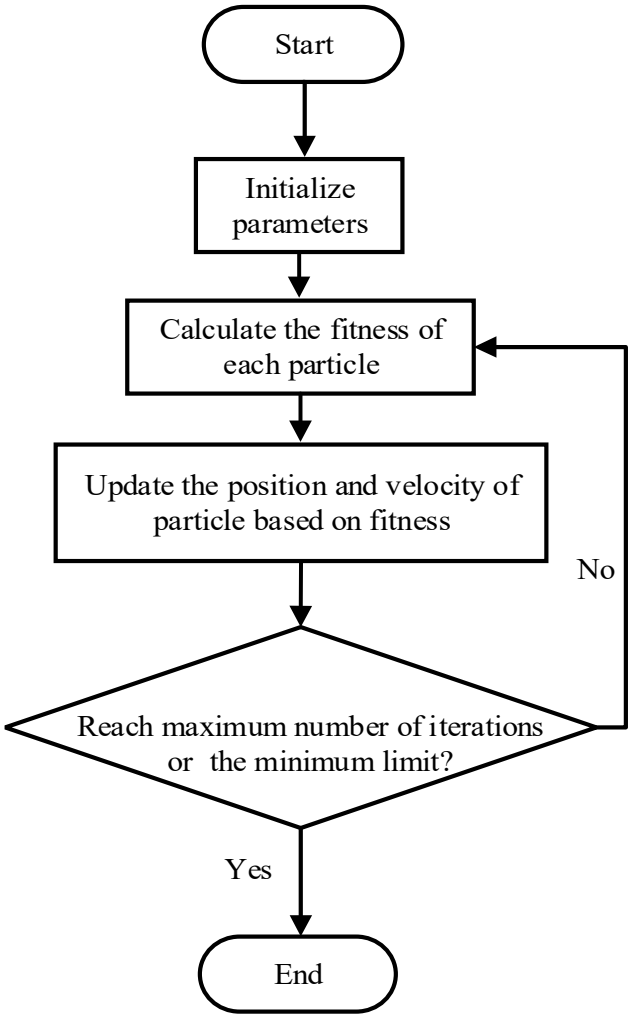

Figure 4. PSO algorithm flowchart.

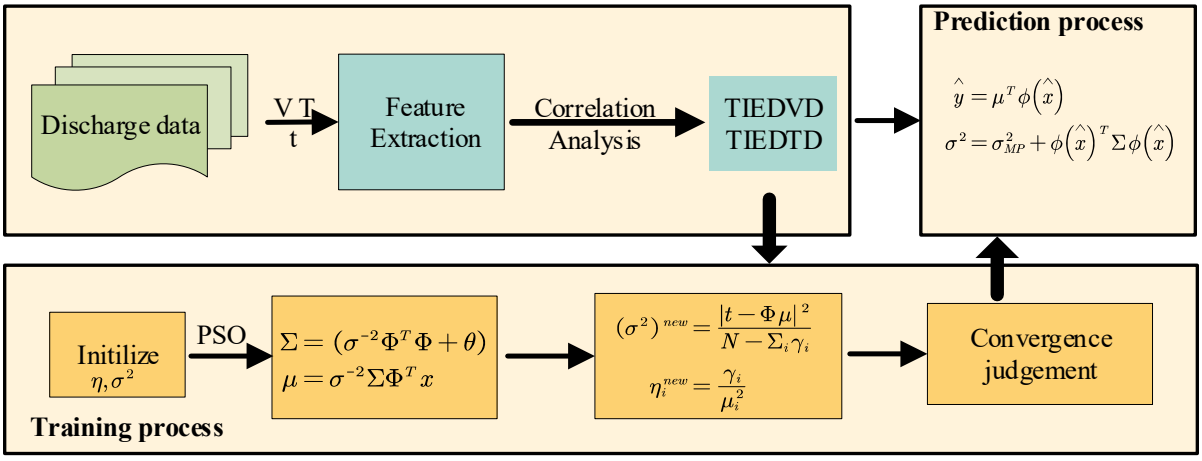

Figure 5. The procedure of the MKRVM.

In Figure 5, the details of battery SOH prognostic are described as follows:

(1) Feature extraction: TIEDVD and TIEDTD are extracted from the discharge data of the lithium-ion battery, $[TIEDVD, TIEDTD] = \begin{bmatrix} TIEDVD_1, TIEDVD_2, \ldots, TIEDVD_n \\ TIEDTD_1, TIEDTD_2, \ldots, TIEDTD_n \end{bmatrix}^T$.

(2) Calculation of the SOH of the battery: $SOH = \frac{C_i}{C_0}$.

(3) Division of the dataset: Divide the dataset into the training set and test set, set the prediction starting point to k; then, the training set input is $x = \begin{bmatrix} TIEDVD_1, TIEDVD_2, \ldots, TIEDVD_k \\ TIEDTD_1, TIEDTD_2, \ldots, TIEDTD_k \end{bmatrix}^T$, the corresponding target variable is $y = [SOH_1, SOH_2, \ldots SOH_k]$, and the test set can be described as $\hat{x} = \begin{bmatrix} TIEDVD_{k+1}, TIEDVD_{k+2}, \ldots, TIEDVD_n \\ TIEDTD_{k+1}, TIEDTD_{k+2}, \ldots, TIEDTD_n \end{bmatrix}^T$, $\hat{y} = [SOH_{k+1}, SOH_{k+2}, \ldots SOH_n]^T$.

(4) Training process: Establish a PSO-MKRVM model and get the optimized weight values. This part detail has been shown in Sections 3.1 and 3.2.

(5) Prediction process: Use the optimized weights to construct a prediction model; the data of the test set in the model for prediction is shown in Equation (14).

(6) Evaluation of prediction results.

3.4. Evaluation Indicators

In order to evaluate the performance of the MKRVM method, root mean square error (RMSE) and mean absolute percentage error (MAPE) act as evaluation indicators in this paper, whose calculation formulas are given as follows:

$$RMSE = \sqrt{\frac{1}{N}\sum_{i=1}^{N}(y_i - \hat{y}_i)^2} \tag{22}$$

$$MAPE = \frac{1}{N}\sum_{i=1}^{N}\left|\frac{y_i - \hat{y}_i}{y_i}\right| \times 100\% \tag{23}$$

where $\hat{y}_i$ denotes the predicted SOH, and y_i denotes the real SOH.

4. Numerical Experiments and Results Analysis

To verify the method proposed in this paper, batteries #5, #6, #7, and #18 are tested to prove the performance of MKRVM and the results with different models at the same starting points are analyzed, while the experiments at different starting points are also carried out. In addition, batteries #54 and #55 are tested with the MKRVM method at different starting points to verify the MKRVM for SOH predictions and analyze the results.

4.1. SOH Prediction at Same Starting Points for Different HIs

In order to present the advantages of the multi-kernel functions, we take the battery #5 as an example, the starting point is cycle 80, and the prediction results of a single TIEDVD, TIEDTD, and the combination of TIEDVD and TIEDTD are compared and shown in Figure 6, while the corresponding RMSE and MAPE are shown in Table 2. It can be seen from Figure 6 and Table 2 that the prediction result of the two HIs combined together is the best, and the RMSE and MAPE are also the smallest, with the values of 0.004 and 0.2932, respectively. The prediction result of TIEDTD is the worst, and the RMSE is 0.0159.

TIEDVD only considers the impact of voltage on capacity degradation, while TIEDTD only considers the influence of temperature on battery degradation. However, the influencing factors of battery degradation are related to both voltage and temperature, so TIEDVD combined with TIEDTD can not only accurately predict the trend but also capture the capacity recovery. Therefore, TIEDVD and TIEDTD are regarded as the inputs of MKRVM to improve the prediction accuracy of SOH in this paper.

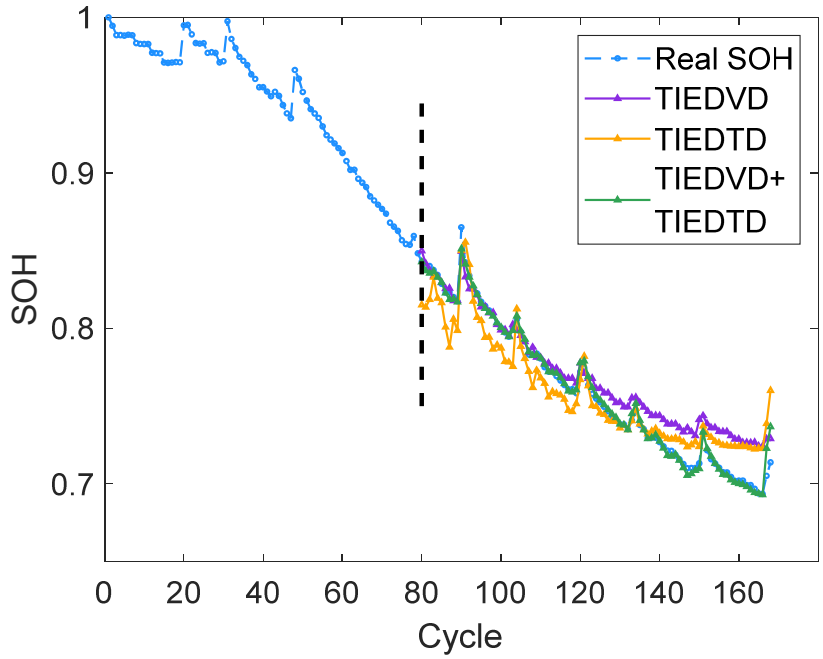

Figure 6. Comparison of different HIs.

Table 2. Prediction RMSE and MAPE for different HIs.

Evaluation Indicators	TIEDVD	TIEDTD	TIEDVD + TIEDTD
RMSE	0.0148	0.0159	0.0040
MAPE	1.5746	1.7532	0.2932

4.2. SOH Prediction at Same Starting Points for Different Models

In order to verify the effectiveness of the MKRVM method, we set up different models at the same starting points and compared them with SVR and GPR models, which are widely used to predict the SOH of lithium-ion batteries. Figure 7 shows the prediction results of SOH by using the proposed method, RVM with Gaussian kernel function, GPR with Gaussian kernel function, and SVR with Gaussian function for four batteries, which are denoted as M1, M2, M3, and M4, respectively. In Figure 7, the start point is cycle 80 for batteries #5, #6, and #7, while the start point is cycle 60 for battery #18. In the comparison experiments, M2 is considered to illustrate the affection of the kernel function in the proposed method, and M3 and M4 are also tested to analyze the affection of RVM in the proposed model.

Figure 7 shows the prediction results of different models for the four batteries, from which one can see that all the four models can predict the trend of SOH well, indicating the advantage of machine learning. However, the results of M2, M3, and M4 deviate from the true value; since multi-kernel functions can learn better than the single kernel function, M3 and M4 can provide better results than M2, which indicates that RVM can be improved a lot. It can be observed from Figure 7 that the prediction results by using MKRVM are close to the actual values and more accurate than those by using other methods, which indicates that MKRVM effectively provides the accurate prediction. Therefore, the results demonstrate that the multi-kernel functions of the proposed method effectively obtain the improved prediction performance.

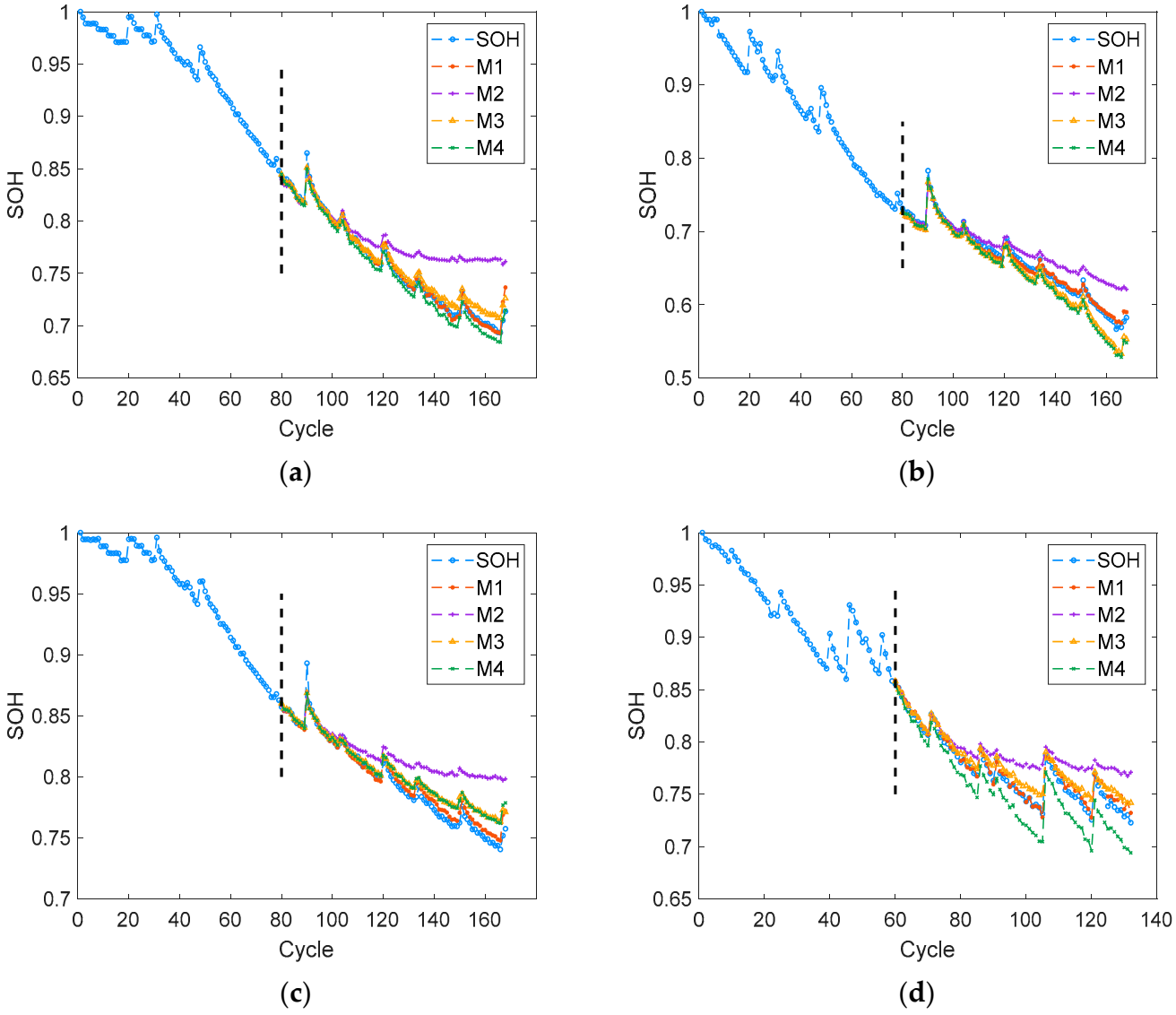

Figure 7. Prediction results on the comparisons for different models. (**a**) #5; (**b**) #6; (**c**) #7; (**d**) #18.

The RMSE and MAPE of SOH prediction results of the four methods are shown in Figure 8. It can be observed from Figure 8 that M1 shows the lowest RMSE and MAPE, which are 0.004 and 0.293, respectively. The comparisons between different models indicate that the proposed method has the best SOH prediction performance among the four methods. It is clear that the MKRVM is highly accurate and effective for SOH prediction. The error comparisons between M1 and M2 indicate that the Gaussian combined with sigmoid multi-kernel functions have better performance than the Gaussian kernel function, which indicates that the proposed method is valid for SOH prediction. The RMSE of M1 is the smallest, and the RMSE of M2 is the largest. Although the RMSEs of M3 and M4 are less than M2, the M3 and M4 models are not sparse, and the M4 model cannot provide probabilistic prediction results. So, we consider improving the M2. The error of M2 is not satisfying; this is because for M2 without a global sigmoid kernel function, and with the MKRVM, which is the improved RVM, the RMSE is the best. It can be observed that the MKRVM method can improve the performance of SOH prediction.

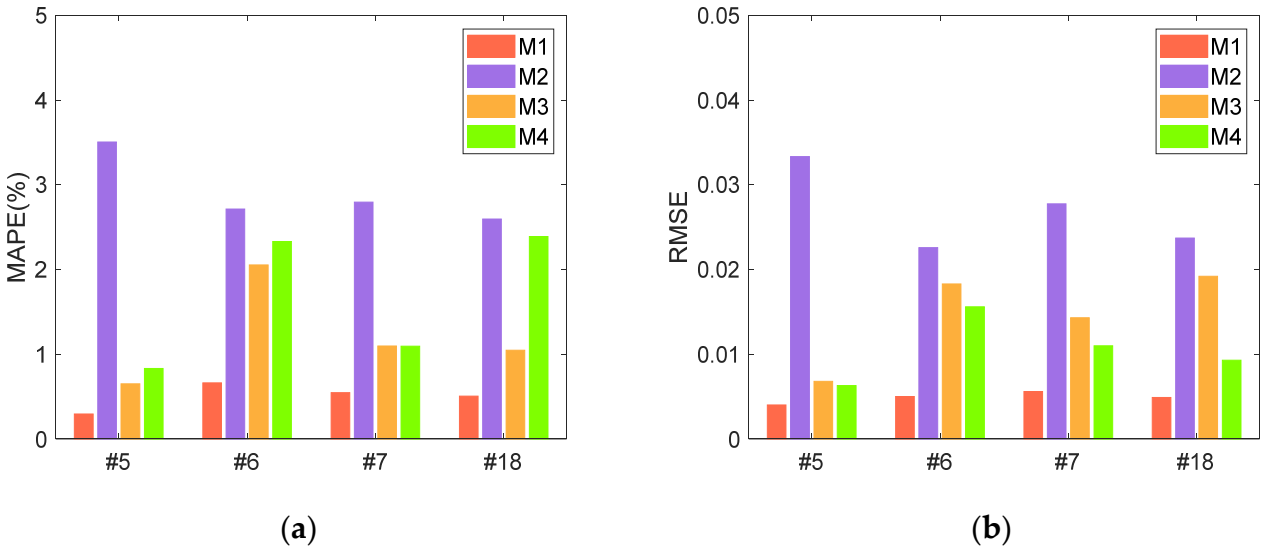

Figure 8. Prediction RMSE and MAPE on the comparisons for different models. (**a**) MAPE; (**b**) RMSE.

4.3. SOH Prediction at Different Starting Points for the Same Model

In order to verify the generalization ability of the MKRVM, the SOH prediction of batteries #5, #6, #7, and #18 at different starting points are tested, whose results are presented in Figure 9. In numerical experiments, the starting points for batteries #5, #6, and #7 are 60, 80, and 100, respectively, while the starting points for batteries #18, #54, and #55 are 40, 60, and 80, respectively. Moreover, the SOH prediction errors are shown in Figure 9b,d,f,h; it is clear that the errors of SOH prediction are very low, which indicates that the accuracy of the MKRVM method is high. It can be observed that the proposed method can predict the SOH accurately in general. For instance, the prediction of battery #5 is similar to the actual value, which demonstrates that the MKRVM method can effectively obtain more accurate prediction results. It is also shown that the predictions at the later time point are close to actual values; the reason is that the earlier the forecast starting point can be set up, the more historical information can be tested to build the model. In addition, the late period predictions are more important than the early ones for battery health management. The SOH prediction in the later period can provide us with guidance on when to replace the battery. However, the prediction errors from different starting points are very small, and it can be concluded that the proposed method in this paper shows higher reliability and strong generalization ability, which can be attributed to the multi-kernel functions and the extracted HIs.

To verify the effectiveness of the MKRVM method for the SOH prediction of batteries at different temperatures, batteries #54 and #55 that operate at low temperature are further used for SOH prediction. Batteries #54 and #55 have capacity recovery phenomena during the degradation process and present various local fluctuations. Figure 9 presents SOH results and errors on the two batteries; it can be observed from Figure 9 that the predictions of the proposed method are close to the true value, which can capture the local fluctuations and especially at the change points. This indicates that the proposed method can provide effective SOH prediction when there are many local regenerations in the battery capacity. Moreover, the SOH errors are kept in a certain range, which demonstrates that the MKRVM method is able to improve the prediction accuracy of the proposed method.

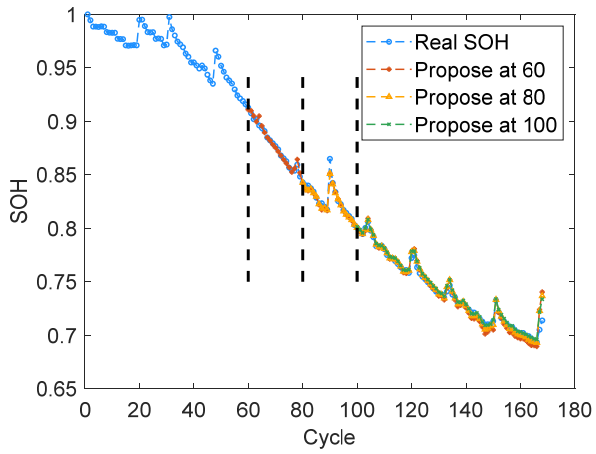

(**a**)

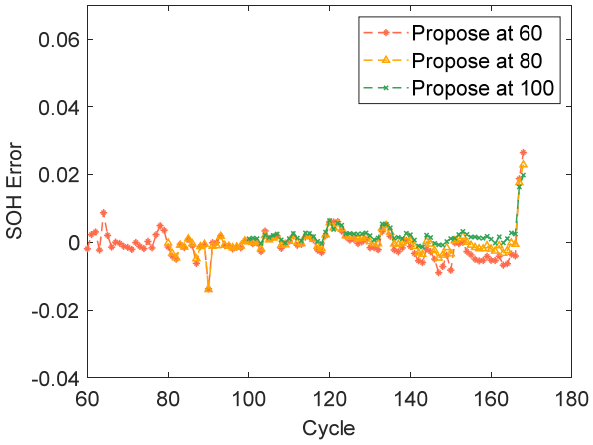

(**b**)

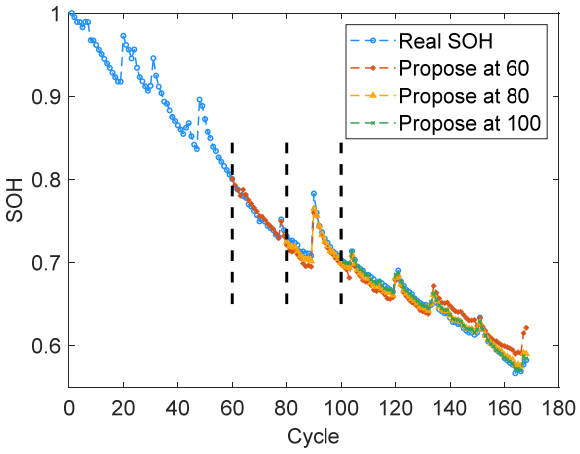

(**c**)

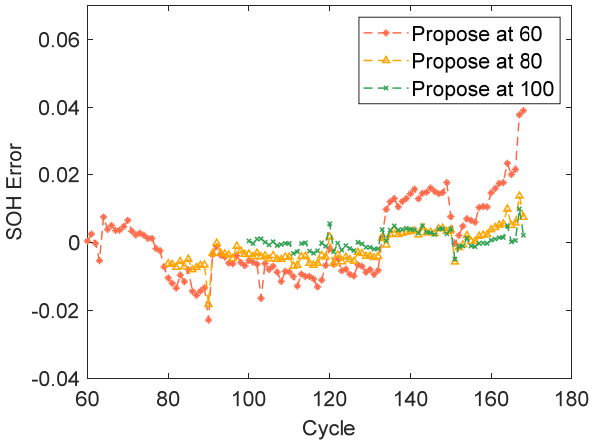

(**d**)

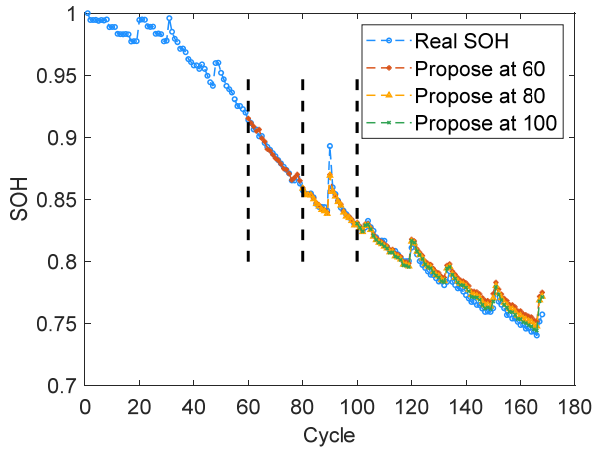

(**e**)

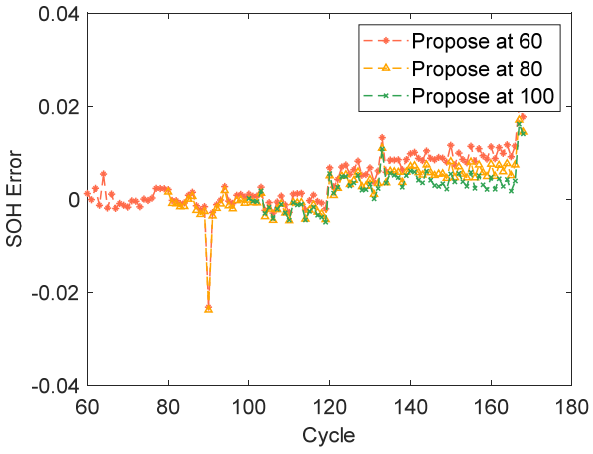

(**f**)

Figure 9. *Cont*.

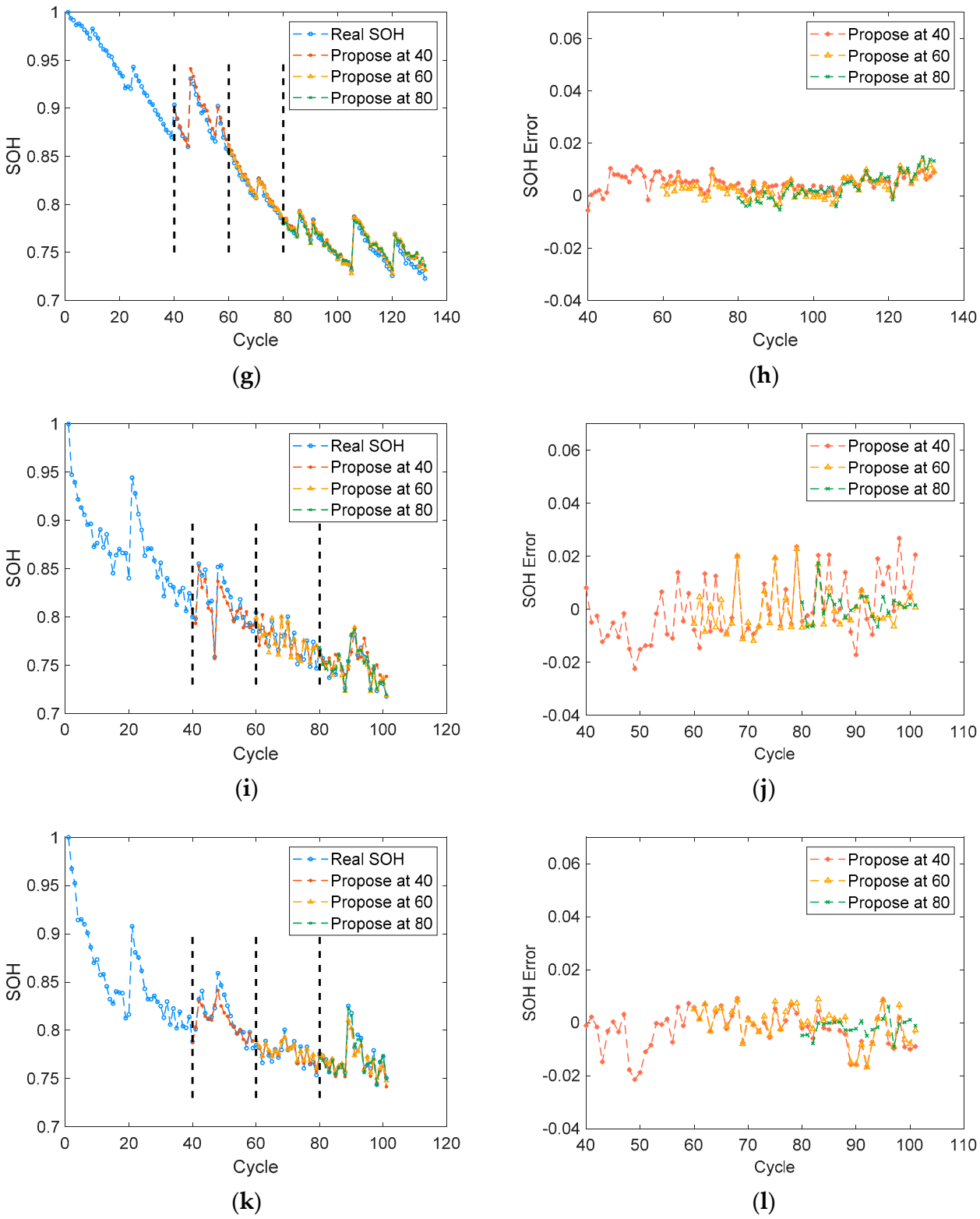

Figure 9. Prediction results on different testing batteries at different starting points; (**a**,**b**) #5; (**c**,**d**) #6; (**e**,**f**) #7; (**g**,**h**) #18; (**i**,**j**) #54; (**k**,**l**) #55.

Table 3 shows the RMSE and MAPE of different starting points. The MAPE of battery #5 is the smallest among the four batteries. The RMSE of different starting points of the MKRVM approach is controlled below 0.01, and we obtain the minimum RMSE and MAPE, which are 0.0027 and 0.29%, and the maximum MAPE is less than 0.4%. Other batteries

also follow a similar trend. The largest RMSE and MAPE of the proposed method among four batteries are 0.0115 and 1.457%, respectively. In addition, the prediction results change with the different starting points, and the error range of the method proposed in this paper is relatively small. It can be concluded that the accuracy of the model proposed in this paper is high.

Table 3. Prediction RMSE and MAPE on comparisons for different starting points.

Battery	Starting Prediction Point	RMSE	MAPE (%)
#5	60	0.0047	0.3956
	80	0.004	0.2932
	100	0.0039	0.3262
#6	60	0.0115	1.457
	80	0.0051	0.6616
	100	0.0027	0.3235
#7	60	0.0067	0.6241
	80	0.0056	0.5462
	100	0.0046	0.4861
#18	40	0.0056	0.6155
	60	0.005	0.506
	80	0.0048	0.6338
#54	40	0.0118	1.2707
	60	0.0082	0.853
	80	0.0052	0.5147
#55	40	0.0078	0.7259
	60	0.0066	0.6772
	80	0.0036	0.3263

Moreover, the RMSE and MAPE results of batteries #54 and #55 are also shown in Table 3. It can be observed that the results of SOH prediction in low temperature have a smaller prediction error with the proposed method, which indicates the ability of the multi-kernel functions. In addition, it is also noted that the performance of the extracted HIs are valid. Although batteries #54 and #55 have many local fluctuations, the prediction results can follow this fluctuation, which proves that the proposed method is still effective for SOH prediction when the temperature changes or has many local fluctuations.

5. Conclusions

We propose a method to predict the SOH of lithium-ion batteries based on changes in discharge voltage and temperature in this paper. The voltage and temperature extracted from the discharge process can be used for online prediction. Then, the MKRVM model is improved based on the basic RVM model in terms of the kernel function design in order to improve the SOH estimate accuracy, and the PSO algorithm is used to optimize the parameters of the MKRVM. The experimental results of different models of batteries #5, #6, #7, and #18 show that the method proposed in this paper has higher accuracy than the other methods, the experimental results of batteries #5–#18 and batteries #54 and #55 at different starting points show that the method presented in this paper has high accuracy.

The further works can be considered as follows: (1) The study of long-term SOH prediction for other kinds of batteries based on MKRVM due to that long-term SOH prediction is of great significance to the preventive management of batteries; (2) The design of more accurate SOH prediction methods by optimizing the current model; (3) The study of an adaptive kernel function of MKRVM for lithium-ion batteries by reducing the calculation time. (4) We will utilize the random datasets, which are continuously cycled with randomly generated current profiles, to verify the effectiveness of the proposed method in our future work.

Author Contributions: Conceptualization, Y.Y. and J.W.; methodology, Y.Y. and J.W.; software, Y.Y.; validation, Y.Y. and J.W. formal analysis, Y.Y.; investigation, Y.Y. and J.W.; writing—original draft preparation, Y.Y.; writing—review and editing, J.W.; visualization, Y.Y.; supervision, J.W., Y.S. and J.Z.; project administration, J.W., Y.S. and J.Z.; funding acquisition, J.W., Y.S. and J.Z. All authors have read and agreed to the published version of the manuscript.

Funding: This research was funded by the National Natural Science Foundation of China, grant number 61533013, the Natural Science Foundation of Shanxi Province, grant number 201801D221208, the Scientific and Technological Innovation Programs of Higher Education Institutions in Shanxi, grant number 2019L0583, the key Program of Research and Development of Shanxi Province, grant number 201703D111011 and the Postgraduate Science and Technology Project of North University of China, grant number 20201770.

Data Availability Statement: No new data were created or analyzed in this study. Data sharing is not applicable to this article.

Acknowledgments: The authors would like to thank the NASA Ames Center of Excellence Diagnostic Center for providing the experimental data.

Conflicts of Interest: The authors declare no conflict of interest.

References

1. Wang, C.S.; Lu, N.Y.; Wang, S.L.; Cheng, Y.H.; Jiang, B. Dynamic Long Short-Term Memory Neural-Network-Based Indirect Remaining-Useful-Life Prognosis for Satellite Lithium-Ion Battery. *Appl. Sci.* **2018**, *8*, 2078. [CrossRef]
2. Hu, C.; Ye, H.; Jain, G.; Schmidt, C. Remaining useful life assessment of lithium-ion batteries in implantable medical devices. *J. Power Sources* **2018**, *375*, 118–130. [CrossRef]
3. Ungurean, L.; Carstoiu, G.; Micea, M.V.; Groza, V. Battery state of health estimation: A structured review of models, methods and commercial devices. *Int. J. Energy Res.* **2017**, *41*, 151–181. [CrossRef]
4. Zhou, Y.P.; Huang, M.H. Lithium-ion batteries remaining useful life prediction based on a mixture of empirical mode decomposition and ARIMA model. *Microelectron. Reliab.* **2016**, *65*, 265–273. [CrossRef]
5. Wu, L.F.; Fu, X.H.; Guan, Y. Review of the Remaining Useful Life Prognostics of Vehicle Lithium-Ion Batteries Using Data-Driven Methodologies. *Appl. Sci.* **2016**, *6*, 166. [CrossRef]
6. Mosallam, A.; Medjaher, K.; Zerhouni, N. Data-driven prognostic method based on Bayesian approaches for direct remaining useful life prediction. *J. Intell. Manuf.* **2016**, *27*, 1037–1048. [CrossRef]
7. Liao, L.X.; Kottig, F. Review of Hybrid Prognostics Approaches for Remaining Useful Life Prediction of Engineered Systems, and an Application to Battery Life Prediction. *IEEE Trans. Reliab.* **2014**, *63*, 191–207. [CrossRef]
8. Hu, X.; Li, S.; Peng, H. A comparative study of equivalent circuit models for Li-ion batteries. *J. Power Sources* **2012**, *198*, 359–367. [CrossRef]
9. Zhang, L.; Zhongqiang, M.; Sun, C.-Y. Remaining Useful Life Prediction for Lithium-Ion Batteries Based on Exponential Model and Particle Filter. *IEEE Access* **2018**, *6*, 17729–17740. [CrossRef]
10. Lyu, C.; Lai, Q.Z.; Ge, T.F.; Yu, H.H.; Wang, L.X.; Ma, N. A lead-acid battery's remaining useful life prediction by using electrochemical model in the Particle Filtering, framework. *Energy* **2017**, *120*, 975–984. [CrossRef]
11. Liu, J.; Chen, Z.Q. Remaining Useful Life Prediction of Lithium-Ion Batteries Based on Health Indicator and Gaussian Process Regression Model. *IEEE Access* **2019**, *7*, 39474–39484. [CrossRef]
12. Li, L.L.; Wang, P.C.; Chao, K.H.; Zhou, Y.T.; Xie, Y. Remaining Useful Life Prediction for Lithium-Ion Batteries Based on Gaussian Processes Mixture. *PLoS ONE* **2016**, *11*, e0163004. [CrossRef]
13. Liu, H.P.; Wu, J.J.; Ye, X.; Liao, T.J.; Chen, M.L. A method based on Dempster-Shafer theory and support vector regression-particle filter for remaining useful life prediction of crusher roller sleeve. *Mech. Ind.* **2019**, *20*, 106. [CrossRef]
14. Yang, W.A.; Xiao, M.H.; Zhou, W.; Guo, Y.; Liao, W.H. A Hybrid Prognostic Approach for Remaining Useful Life Prediction of Lithium-Ion Batteries. *Shock Vib.* **2016**, *2016*, 3838765. [CrossRef]
15. Liu, D.T.; Zhou, J.B.; Pan, D.W.; Peng, Y.; Peng, X.Y. Lithium-ion battery remaining useful life estimation with an optimized Relevance Vector Machine algorithm with incremental learning. *Measurement* **2015**, *63*, 143–151. [CrossRef]
16. Zhang, Y.Z.; Xiong, R.; He, H.W.; Pecht, M.G. Long Short-Term Memory Recurrent Neural Network for Remaining Useful Life Prediction of Lithium-Ion Batteries. *IEEE Trans. Veh. Technol.* **2018**, *67*, 5695–5705. [CrossRef]
17. Xia, T.B.; Song, Y.; Zheng, Y.; Pan, E.S.; Xi, L.F. An ensemble framework based on convolutional bi-directional LSTM with multiple time windows for remaining useful life estimation. *Comput. Ind.* **2020**, *115*, 103182. [CrossRef]
18. Qu, J.T.; Liu, F.; Ma, Y.X.; Fan, J.M. A Neural-Network-Based Method for RUL Prediction and SOH Monitoring of Lithium-Ion Battery. *IEEE Access* **2019**, *7*, 87178–87191. [CrossRef]
19. Qin, T.; Zeng, S.; Guo, J. Robust prognostics for state of health estimation of lithium-ion batteries based on an improved PSO–SVR model. *Microelectron. Reliab.* **2015**, *55*, 1280–1284. [CrossRef]

20. Zhao, Q.; Qin, X.L.; Zhao, H.B.; Feng, W.Q. A novel prediction method based on the support vector regression for the remaining useful life of lithium-ion batteries. *Microelectron. Reliab.* **2018**, *85*, 99–108. [CrossRef]
21. Widodo, A.; Shim, M.-C.; Caesarendra, W.; Yang, B.-S. Intelligent prognostics for battery health monitoring based on sample entropy. *Expert Syst. Appl.* **2011**, *38*, 11763–11769. [CrossRef]
22. Liu, S.X.; Zhou, Y.F.; Liu, Y.L.; Lian, J.; Huang, L.J. A Method for Battery Health Estimation Based on Charging Time Segment. *Energies* **2021**, *14*, 2612. [CrossRef]
23. Yang, D.; Zhang, X.; Pan, R.; Wang, Y.; Chen, Z. A novel Gaussian process regression model for state-of-health estimation of lithium-ion battery using charging curve. *J. Power Sources* **2018**, *384*, 387–395. [CrossRef]
24. Liu, D.; Zhou, J.; Liao, H.; Peng, Y.; Peng, X. A Health Indicator Extraction and Optimization Framework for Lithium-Ion Battery Degradation Modeling and Prognostics. *IEEE Trans. Syst. Man Cybern. Syst.* **2015**, *45*, 915–928. [CrossRef]
25. Yang, H.; Xu, Z.; Ye, J.; King, I.; Lyu, M.R. Efficient Sparse Generalized Multiple Kernel Learning. *IEEE Trans. Neural Netw.* **2011**, *22*, 433–446. [CrossRef]
26. Blekas, K.; Likas, A. Sparse regression mixture modeling with the multi-kernel relevance vector machine. *Knowl. Inf. Syst.* **2014**, *39*, 241–264. [CrossRef]
27. Zhang, C.; He, Y.; Yuan, L.; Xiang, S. Capacity Prognostics of Lithium-Ion Batteries Using EMD Denoising and Multiple Kernel RVM. *IEEE Access* **2017**, *5*, 12061–12070. [CrossRef]
28. Xue, Z.W.; Zhang, Y.; Cheng, C.; Ma, G.J. Remaining useful life prediction of lithium-ion batteries with adaptive unscented kalman filter and optimized support vector regression. *Neurocomputing* **2020**, *376*, 95–102. [CrossRef]
29. Wei, J.W.; Dong, G.Z.; Chen, Z.H. Remaining Useful Life Prediction and State of Health Diagnosis for Lithium-Ion Batteries Using Particle Filter and Support Vector Regression. *IEEE Trans. Ind. Electron.* **2018**, *65*, 5634–5643. [CrossRef]
30. Dong, H.; Jin, X.; Lou, Y.; Wang, C. Lithium-ion battery state of health monitoring and remaining useful life prediction based on support vector regression-particle filter. *J. Power Sources* **2014**, *271*, 114–123. [CrossRef]
31. Tang, X.; Wang, Y.; Zou, C.; Yao, K.; Xia, Y.; Gao, F. A novel framework for Lithium-ion battery modeling considering uncertainties of temperature and aging. *Energy Convers. Manag.* **2019**, *180*, 162–170. [CrossRef]
32. Ma, S.; Jiang, M.; Tao, P.; Song, C.; Wu, J.; Wang, J.; Deng, T.; Shang, W. Temperature effect and thermal impact in lithium-ion batteries: A review. *Prog. Nat. Sci. Mater. Int.* **2018**, *28*, 653–666. [CrossRef]
33. Ruiz, V.; Kriston, A.; Adanouj, I.; Destro, M.; Fontana, D.; Pfrang, A. Degradation Studies on Lithium Iron Phosphate–Graphite Cells. The Effect of Dissimilar Charging—Discharging Temperatures. *Electrochim. Acta* **2017**, *240*, 495–505. [CrossRef]
34. Yu, J. State of health prediction of lithium-ion batteries: Multiscale logic regression and Gaussian process regression ensemble. *Reliab. Eng. Syst. Saf.* **2018**, *174*, 82–95. [CrossRef]
35. Saha, B.; Goebel, K. Battery Data Set. Available online: http://ti.arc.nasa.gov/tech/dash/pcoe/prognostic-data-repository/ (accessed on 18 February 2020).
36. Li, X.; Wang, Z.; Yan, J. Prognostic health condition for lithium battery using the partial incremental capacity and Gaussian process regression. *J. Power Sources* **2019**, *421*, 56–67. [CrossRef]
37. dos Reis, G.; Strange, C.; Yadav, M.; Li, S. Lithium-ion battery data and where to find it. *Energy AI* **2021**, *5*, 100081. [CrossRef]
38. Chinomona, B.; Chung, C.; Chang, L.-K.; Su, W.-C.; Tsai, M.-C. Long Short-Term Memory Approach to Estimate Battery Remaining Useful Life Using Partial Data. *IEEE Access* **2020**, *8*, 165419–165431. [CrossRef]
39. Zhou, D.; Xue, L.; Song, Y.; Chen, J. On-Line Remaining Useful Life Prediction of Lithium-Ion Batteries Based on the Optimized Gray Model GM(1,1). *Batteries* **2017**, *3*, 21. [CrossRef]
40. Yun, Z.; Qin, W. Remaining Useful Life Estimation of Lithium-Ion Batteries Based on Optimal Time Series Health Indicator. *IEEE Access* **2020**, *8*, 55447–55461. [CrossRef]
41. Zheng, X.J.; Fang, H.J. An integrated unscented kalman filter and relevance vector regression approach for lithium-ion battery remaining useful life and short-term capacity prediction. *Reliab. Eng. Syst. Saf.* **2015**, *144*, 74–82. [CrossRef]
42. Liu, Y.F.; Zhao, G.Q.; Peng, X.Y. Deep Learning Prognostics for Lithium-Ion Battery Based on Ensembled Long Short-Term Memory Networks. *IEEE Access* **2019**, *7*, 155130–155142. [CrossRef]